An EMMPRIN/γ-catenin/Nm23 complex drives ATP production and actomyosin contractility at endothelial junctions

Vanessa Moreno[1], Pilar Gonzalo[1], Jesús Gómez-Escudero[1], Ángela Pollán[1], Rebeca Acín-Pérez[1], Mark Breckenridge[2], María Yáñez-Mó[4], Olga Barreiro[1], Fabrizio Orsenigo[3], Kenji Kadomatsu[5], Christopher S. Chen[2], José A. Enríquez[1], Elisabetta Dejana[3], Francisco Sánchez-Madrid[4], and Alicia G. Arroyo[1]

[1]Centro Nacional de Investigaciones Cardiovasculares (CNIC), 28029 Madrid, Spain.

[2] University of Pennsylvania, Philadelphia, PA 19104, USA.

[3] FIRC Institute of Molecular Oncology, University of Milan, 20139 Milan, Italy.

[4]Instituto de Investigación Sanitaria Princesa. Universidad Autónoma de Madrid, 28006 Madrid, Spain.

[5] Nagoya University, Nagoya, 464-8601, Japan.

Corresponding author

Alicia G. Arroyo, MD, PhD

Matrix metalloproteinase lab

Vascular Biology & Inflammation Department

Centro Nacional de Investigaciones Cardiovasculares (CNIC)

Melchor Fernández Almagro 3

28029 Madrid

Spain

Phone 34 91 4531241 ext 1159

FAX 34 91 4531265

e-mail agarroyo@cnic.es

Running title: EMMPRIN in endothelial junction

Keywords: EMMPRIN; endothelial junctions; γ-catenin; Nm23 (nucleoside diphosphate kinase, NDPK); ATP; actomyosin contractility; vascular integrity

JCS Advance Online Article. Posted on 2 July 2014

SUMMARY

Cell-cell adhesions are important sites through which cells experience and resist forces. In endothelial cells, these forces regulate junction dynamics and determine endothelial barrier fitness. We identify the Ig superfamily member EMMPRIN as a coordinator of forces at endothelial junctions. EMMPRIN location at junctions correlates with endothelial junction strength at different mouse vascular beds. Accordingly, EMMPRIN-deficient mice show altered junctions and increased permeability. Lack of EMMPRIN alters VE-cadherin pattern and function by decreasing actomyosin contractility and tugging forces at endothelial cell junctions. EMMPRIN ensures proper actomyosin-driven maturation of competent endothelial junctions by forming a molecular complex with γ-catenin and Nm23, a nucleoside diphosphate kinase, thereby locally fueling ATP to the actomyosin machinery. These results provide a novel mechanism for regulation of actomyosin contractility at endothelial junctions and might have broader implications in biological contexts such as angiogenesis, collective migration and tissue morphogenesis by coupling compartmentalized energy production to junction assembly.

INTRODUCTION

A fundamental issue in vascular biology is the understanding of the mechanisms that govern vessel stabilization since it is required for development and growth of the organism and since changes in vessel permeability contribute to several pathologies. Vascular integrity depends on the assembly of multicomponent endothelial junctions, the most extensively studied being homophilic VE-cadherin interactions at adherens junctions (AJs) (Dejana, 2004; Giannotta et al., 2013); however the complete molecular map of the assembly and disassembly of these junctions remains to be defined. Endothelial dynamics largely depends on the spatiotemporal reorganization of the actin cytoskeleton during AJ maturation (Smutny et al., 2010) and on the tension that actin filaments in conjunction with non-muscle myosin II (NM-II) exert over the membrane. This tension actively participates in the expansion from single, unstable intercellular cadherin interactions, to stable cell contacts involving multiple cadherin pairings (Baum and Georgiou, 2011; Mege et al., 2006; Smutny et al., 2010). Although it is known that non-muscle myosin II (NM-II) contributes to generate this tension required for proper maintenance of linear AJs through several mechanisms (Mege et al., 2006), the spatiotemporal regulation of NM-II-driven tension at cell-cell junctions is just beginning to be elucidated especially in endothelial monolayers, which experience stronger shear and flow forces than epithelial barriers (Abraham et al., 2009; Ando et al., 2013; Baum and Georgiou, 2011; Conway et al., 2013; Huveneers et al., 2012; Wimmer et al., 2012).

EMMPRIN (extracellular matrix metalloproteinase inducer, also called basigin and CD147) is a glycosylated type I transmembrane protein of the Ig superfamily (Muramatsu and Miyauchi, 2003), and EMMPRIN molecules are therefore able to engage in homophilic interactions with other monomers and in heterophilic interactions with other partners, such as monocarboxylate transporters, integrins, caveolin-1, CD98, cyclophilins, and Shrew1 (Berditchevski et al., 1997; Deora et al., 2005; Schreiner et al., 2007; Tang and Hemler, 2004; Xu and Hemler, 2005). EMMPRIN function has mostly been characterized in relation to tumorigenesis and inflammation (Muramatsu and Miyauchi, 2003). EMMPRIN can also contribute to angiogenesis, the formation of new vessels, by endothelial cell activation when present on tumor-derived microvesicles (Millimaggi et al., 2007); by regulation of the PI3K/Akt signaling pathway in activated endothelial cells (Chen et al.,

2009); and by modulating the secretion of specific VEGF isoforms (Bougatef et al., 2009). Whether EMMPRIN plays additional roles in the quiescent vasculature has not been investigated.

Here, we report that EMMPRIN orchestrates junction stability in vitro and in vivo by forming a novel molecular complex at endothelial junctions with γ-catenin and the nucleoside diphosphate kinase Nm23, which provides ATP for the local actomyosin contractility required for proper junction maturation.

RESULTS

Endothelial junctions are altered and vascular permeability enhanced in EMMPRIN-deficient mice

Analysis of mouse tissue sections revealed colocalization of EMMPRIN with the endothelial cell junction marker PECAM-1 in the continuous non-fenestrated endothelium of heart and lung vessels and in the specialized tight endothelium of the blood-brain barrier, but not in the continuous fenestrated endothelium of kidney glomeruli and spleen, a pattern indicating a correlation between EMMPRIN expression and junction strength (Supplementary Fig. S1A). In whole-mount specimens, EMMPRIN was also detected at the junctions of the microvasculature of the ear and at the endothelium of large vessels (aorta) (Supplementary Fig. S1B).

Enrichment in EMMPRIN at endothelial cell-cell junctions of different vascular beds suggests a function at these sites. We therefore analyzed the vasculature of EMMPRIN-deficient mice. EMMPRIN null mice show no apparent vascular defect, and skin and organ coloration is similar to wild-types, indicating no hemorrhage or gross alterations to irrigation. However, ex vivo whole mount staining for the junction marker PECAM-1 revealed altered intercellular contacts in several vascular territories. In the microvasculature of the trachea and the ear, the cell boundary PECAM-1 staining in EMMPRIN-deficient mice was diffuse and discontinuous compared with the sharp pattern observed in wild-type mice, especially at branch points, where the vessels also appeared to be dilated (Fig. 1A). A similar PECAM-1 phenotype was observed in the tracheal microvasculature of EMMPRIN heterozygous mice, indicating that a full EMMPRIN gene dose is required for proper junction formation (unpublished data). The pattern of PECAM-1 staining was also subtly irregular in straight, large vessels of the ear and in aortas from EMMPRIN null mice (Fig. 1A).

EMMPRIN null mice do not display macroscopic edema, and skin tone recovery after pressure application was comparable to wild-types; moreover, histological skin sections showed no signs of edema. Nonetheless, given the altered endothelial junction structure in EMMPRIN null mice, we directly explored vessel integrity in vivo by injected animals with Evans Blue. We observed greater accumulation of Evans Blue in the inflamed ears (after application of mustard oil) of EMMPRIN null mice than in their wild-type

counterparts (Fig. 1B); Evans Blue leakage in the inflamed ear was also significantly higher than normal in EMMPRIN heterozygous mice (unpublished data). As a complementary approach, we monitored the tissue leakage of fluorescently labeled low or high molecular weight dextran (4kDa or 70 kDa) by confocal microscopy. Leakage of both molecular weight dextrans was higher in the ears of EMMPRIN null mice when compared to wild-type ears in basal conditions and upon inflammation induced by aural application of mustard oil (Fig. 1C).

EMMPRIN knockdown impairs stability of adherens junctions

Confocal analysis confirmed that EMMPRIN is also located at junctions formed by human umbilical vein endothelial cells (HUVEC), where it partially colocalizes with the junction components VE-cadherin (48% colocalization), PECAM-1 (95%) and JAM-A (81%) (unpublished data). We next investigated how adherens junctions were affected by EMMPRIN deficiency in human ECs. siRNA-mediated interference in EMMPRIN expression with two independent oligonucleotides efficiently decreased protein expression for up to 72 h in culture (Fig. 2A). Immunostaining for endothelial junction components in EMMPRIN-silenced HUVEC revealed a marked alteration in the VE-cadherin pattern. In non-transfected (control) cells or cells transfected with a non-specific siRNA (Neg), VE-cadherin traced well-defined sharp contours at endothelial cell-cell contacts; in contrast, a broader, irregular pattern was detected at most contacts between EMMPRIN-silenced cells (Fig. 2B). Image analysis confirmed a significantly wider peak of VE-cadherin intensity at the borders of EMMPRIN-interfered cells (Fig. 2C). A similarly broadened distribution was observed for the VE-cadherin partner β-catenin (unpublished data). These structural alterations resulted in impaired barrier function as shown by the significantly higher permeability of EMMPRIN-interfered HUVEC monolayers to labeled dextran in transwell assays (Fig. 2D). The function of EMMPRIN in endothelial cell-cell junctions was independently demonstrated in EMMPRIN-deficient primary mouse lung endothelial cells (MLEC), which also displayed reduced intensity, worse definition and overall broadened VE-cadherin distribution at cell-cell junctions (Fig. 2E; Supplementary Figs S2E,F).

EMMPRIN regulates actomyosin-dependent contractility and forces at endothelial junctions

VE-cadherin stability of adherens junctions is related to the tension exerted by circumferential actin bundles together with non-muscle myosin II (NM-II) at these sites (Hoelzle and Svitkina, 2012; Liu et al., 2010). We first observed that EMMPRIN colocalized with F-actin (phalloidin staining) at filopodia and lamellipodia during both early exploratory immature cell-cell contacts (1 h) and mature junctions established over 48 h (Fig. 3A). Branched actin network of immature endothelial junctions (Hoelzle and Svitkina, 2012) was detected at junctions formed by control non-interfered ECs after 1 h whereas junctions in EMMPRIN-interfered cells lacked this branched actin pattern at this early stage and were characterized by the persistence of radial actin filaments (Fig. 3B). To visualize the impact of EMMPRIN deficiency on live actin polymerization during both cell-cell contact formation and maturation, we first interfered human ECs for EMMPRIN, transfected them with LifeAct and then stained them with a directly-labeled anti-EMMPRIN antibody. Time lapse videomicroscopy revealed colocalization of polymerized actin and EMMPRIN clusters at membrane contacts established by non-interfered endothelial cells (Fig. 3C and Supplementary Video 1). In these cells, actin transited from a branched network—with few filaments perpendicular to the junction (see also Fig. 3B)—to parallel filaments as previously described (Mege et al., 2006). In contrast, in EMMPRIN-interfered cells the actin filaments mostly remained perpendicular to the junction (see also Fig. 3B) until the end of the sequence (8:20 h of time lapse videomicroscopy, 24 h after seeding; Fig. 3C and Supplementary Video 2).

To further define actomyosin activity at endothelial junctions, we quantified active non-muscle myosin II (NM-II) (by staining the phosphorylated regulatory myosin light chain; pMLC) and polymerized F-actin (by phalloidin staining) at cellular regions of interest defined around the junctions (ROIs; see Fig. 4A,B and M&M for details). EMMPRIN-interfered human ECs displayed reduced actomyosin activity at the junctions as shown by the significantly decreased staining of pMLC and F-actin, contrasting with the pMLC punctate staining and F-actin enrichment observed at the junctions of control cells (Fig. 4A and 4C). This reduction was further demonstrated by the significant decrease in pMLC/MLC ratio observed by western blot in membrane-enriched fractions from

EMMPRIN-interfered human ECs compared to controls (Fig. 4D). Moreover, a similar reduction of pMLC and F-actin and therefore actomyosin activity was also found at the aortic endothelial junctions of EMMPRIN null mice analyzed ex vivo; this reduction was better visualized in 3D-rendering reconstruction of pMLC and F-actin images (Fig. 4Eand 4F). We next quantified the linearity index (defined by the ratio of junction length to the distance between vertices) introduced by Takeichi's group in epithelial cells as a read-out of actomyosin contractility (Otani et al., 2006); as shown in Fig. 4G, VE-cadherin-based linearity index was significantly increased in EMMPRIN-interfered human ECs compared to control cells demonstrating reduced actomyosin contractility in the absence of EMMPRIN. To directly quantify the forces exerted by actomyosin at the endothelial junctions we plated human endothelial cells on an array of fluorescently labeled elastomeric microneedles, which allows quantification of intercellular tugging forces in pairs of cells (Cohen et al., 2013; Liu et al., 2010). Accordingly to image analysis and western blot data (Fig. 4A-D) and to increased linearity index (Fig. 4G), the intensity of tugging forces (the force across the cell junction) was significantly lower in EMMPRIN-interfered cells (Fig. 4H).

We also observed a significant increase of pMLC (but not F-actin) in the interior of EMMPRIN-deficient HUVEC and aortic endothelial cells (Supplementary Fig. S2A). In an attempt to rescue the phenotype through the reestablishment of tension at the junctions, we next analyzed the effect of relaxing the inner non-muscle myosin activity with the inhibitor of Rho kinase Y27632, which only reduces pMLC inside cells leaving intact punctate pMLC staining at junctions (Smutny et al., 2010; Totsukawa et al., 2000). Y27632 restored the linear VE-cadherin pattern and reversed permeability in EMMPRIN-interfered HUVEC to a level similar to that in control-interfered cells (Supplementary Fig. S2B-D); the inhibitor also restored the junction pattern and integrity in EMMPRIN null MLEC (Supplementary Fig. S2E,F).

EMMPRIN associates with γ-catenin at endothelial junctions

The above results indicate that EMMPRIN contributes to pMLC regulation and actomyosin contractility at EC junctions either through direct interaction with the actomyosin machinery or through an adapter protein. To explore this, we used the EMMPRIN cytosolic

tail as bait to search for interacting proteins in epithelial cell lysates. Mass spectrometry of pulled down proteins identified several candidates, including γ-catenin (plakoglobin), a known component of endothelial cell junctions. The association of EMMPRIN with γ-catenin in HUVEC was confirmed by coimmunoprecipitation (Fig. 5A). The immunoprecipitates did not contain VE-cadherin, and γ-catenin colocalized with EMMPRIN in VE-cadherin null mouse ECs pointing to the VE-cadherin independence of this complex (Fig. 5B). EMMPRIN colocalized with γ-catenin at both early exploratory and stable junctions formed by human ECs (Fig. 5C and unpublished data). Moreover, γ-catenin was barely detected by immunostaining in EMMPRIN-interfered ECs particularly at endothelial junctions in spite of no significant differences in γ-catenin protein levels by western blot, , suggesting that EMMPRIN is necessary for proper recruitment of γ-catenin to these sites (Fig. 5C,D). γ-Catenin was also low at cell-cell junctions of the ear vessels from EMMPRIN-null mice, indicating that EMMPRIN contributes to γ-catenin recruitment to endothelial junctions in vivo (Fig. 5E). Microscopy analysis showed that siRNA interference of γ-catenin in human ECs significantly decreased pMLC and F-actin at junctions, in a similar manner to EMMPRIN-interfered cells, confirming the contribution of this complex to pMLC/actomyosin contractility at junctions (Fig. 5F,G).

An EMMPRIN/γ-catenin/Nm23 complex regulates actomyosin contractility at EC junctions through local ATP production

Given that actomyosin contractility requires ATP, we next investigated the possible role at the junction of the reported γ-catenin partner nucleoside diphosphate kinase Nm23 (Aktary et al., 2010), which is able to generate ATP by exchanging phosphate groups from NTP to ADP. The presence of Nm23 in the EMMPRIN molecular complex was confirmed by coimmunoprecipitation from EC lysates (Fig. 6A). In addition, although Nm23 staining was mostly diffuse within ECs, Nm23 could be found colocalizing with EMMPRIN and γ-catenin at specific points in some junctions of confluent human ECs (Fig. 6B); this was better visualized after methanol fixation or saponin treatment to remove Nm23 soluble cytosolic pool (Supplementary Fig. S3A). The interaction of EMMPRIN with γ-catenin and Nm23 was further demonstrated by proximity ligation assay (PLA) that showed positive

signal for EMMPRIN/γ-catenin and for γ-catenin/Nm23 at endothelial cell junctions of confluent HUVEC monolayers (Fig. 6B, lower panels). Moreover, quantification of Nm23 localization at EC junctions showed a significant reduction in both EMMPRIN- or γ-catenin-interfered HUVEC (Fig. 6C), pointing to an essential requirement of EMMPRIN/γ-catenin for Nm23 recruitment to the junctions. To better address this point, we transfected HUVEC with a myristoylated EMMPRIN cytosolic tail in EMMPRIN-interfered cells; we first confirmed that the myristoylated EMMPRIN cytosolic tail was recruited at endothelial cell junctions likely due to cytosolic residues involved in EMMPRIN traffic (Fig. 7A,B; (Deora et al., 2004)). The myristoylated EMMPRIN cytosolic tail rescued the presence of γ-catenin and Nm23 as well as pMLC and F-actin staining at the junctions of EMMPRIN-interfered cells (Fig. 7A,B), indicating that the sole cytosolic EMMPRIN tail anchored to the membrane is able to recruit γ-catenin and Nm23 and that this interaction is essential for proper actomyosin contractility at junctions.

In order to get further mechanistic insights, we next analyzed the impact of decreasing Nm23 on endothelial junction stability. Endothelial cell junctions were disrupted in Nm23-interfered human ECs as indicated by decreased pMLC and altered F-actin at junctions resulting in significantly increased linearity index together with reduced VE-cadherin staining and enhanced endothelial permeability (Fig. 8A-C; Supplementary Fig. S3B,C). Since Nm23 can directly regulate cytoskeleton contractility in *Dictyostelium* by providing ATP to the myosin molecule (Aguado-Velasco et al., 1996), we explored the possible involvement of this mechanism in mammalian ECs by quantifying ATP production at endothelial junctions. We first used the Perceval plasmid to visualize and quantitate ATP/ADP ratios (Berg et al., 2009) at endothelial junctions in the presence of inhibitors of the main sources of ATP production in ECs (glycolysis and mitochondria; see M&M for details). We visualized and quantified ATP/ADP ratios before and after inhibitor treatment and observed that the ATP/ADP ratio at endothelial cell periphery (junctional area) was decreased at a higher extent in EMMPRIN-interfered compared to control-interfered ECs upon inhibitor addition pointing to lower production of ATP in the absence of EMMPRIN at the membrane (Fig. 8D). To assess this point, we directly quantified ATP production in membrane-enriched fractions in the presence of inhibitors of ATPase synthase and adenylate kinase and of GTP and ADP as substrates for Nm23. ATP production in these

conditions was lower in membranes from EMMPRIN-interfered cells than in membranes from control-interfered cells (Fig. 8E). Moreover, an inhibitory anti-Nm23 antibody significantly decreased ATP production by membranes from control human ECs but had only a minor effect in EMMPRIN-interfered cells, indicating that Nm23 makes an essential contribution to ATP production at the membrane in the presence of EMMPRIN (Fig. 8E). Overall these findings point to decreased pMLC and actomyosin contractility and impaired junctions in EMMPRIN-deficient endothelial cells as a result from defective local ATP production.

DISCUSSION

Our results show that EMMPRIN is essential for endothelial junction stability and vascular integrity. EMMPRIN, through a newly-identified association with γ-catenin and Nm23 during junction formation, acts as a key intermediary between the plasma membrane and actomyosin contractility by providing ATP, thus coordinating the forces required for junction initiation, stabilization and integrity in vitro and in vivo (Supplementary Fig. S4). Endothelial cell-cell adhesions are essential for vascular integrity and their alteration results in severe disorders (Dejana et al., 2009). In spite of no previous vascular phenotype described in EMMPRIN null mice (Muramatsu and Miyauchi, 2003), we observe that they show above-normal vascular leakage under basal and inflammatory conditions, demonstrating an essential contribution of EMMPRIN to endothelial barrier functioning in vivo. This permeability phenotype is unlike that of mice deficient for other Ig family members present at endothelial junctions such as PECAM-1 or JAM-C (Graesser et al., 2002; Orlova et al., 2006), suggesting that each junction component has selective and specific functions in the regulation of vessel integrity. Since permeability differences in arteries, capillaries and venules correlate with the heterogeneous actin organization and function in these vascular beds (Prasain and Stevens, 2009), it is also possible that EMMPRIN contributes to this heterogeneity through its preferential expression at the junctions of certain vascular beds, in particular at those with a tighter endothelial barrier. Forces generated at cell-cell junctions through dynamic interactions between transmembrane proteins and the actomyosin cytoskeleton are especially important for the maintenance of endothelial barrier fitness, but the underlying molecular mechanisms were not fully understood. We identify EMMPRIN as an essential coordinator of these forces since in its absence actomyosin-driven contractility is reduced and VE-cadherin contacts are not properly established; in this regard, we have extended the utility and complementarity (to quantification of junctional pMLC and F-actin by image analysis) of the linearity index as a read-out of actomyosin contractility not only in epithelial but also in endothelial junctions (Otani et al., 2006) Direct quantification by elastomer sensors (Liu et al., 2010) revealed that forces across cell-cell junctions (tugging forces) are significantly diminished in EMMPRIN-interfered ECs. Since this method only allows force quantification in EC pairs it will be of interest to use alternative approaches such as the

recently established FRET-based tension sensors to quantitate junctional forces in established endothelial monolayers (Conway et al., 2013). The relevance of balanced forces for endothelial junction integrity is further supported by the rescue of the wild-type junction phenotype in EMMPRIN-deficient cells upon relaxation of inward tension with a Rho kinase inhibitor.

This function of EMMPRIN in orchestrating spatiotemporal junctional actomyosin (pMLC and F-actin) contractility is particularly relevant since this network is just beginning to be elucidated in ECs (Ando et al., 2013; Huveneers et al., 2012; Wimmer et al., 2012). EMMPRIN absence resulted in delayed actin maturation at endothelial junctions in accordance with its role in organizing cortical actin at neuromuscular junctions in *Drosophila* (Besse et al., 2007). In terms of the mechanism involved, the polybasic juxtamembrane region of EMMPRIN was important for cortical actin organization in *Drosophila*, but no EMMPRIN cytosolic interactions were described except an association with the microtubule protein Hook1 reported recently (Besse et al., 2007; Maldonado-Baez et al., 2013). We identify by mass spectrometry a novel molecular interaction of the cytosolic tail of EMMPRIN with γ-catenin, being this complex required for proper actomyosin-dependent forces during the formation of endothelial junctions. This is in line with the specific role of γ-catenin in organizing the cortical actin skeleton described in *Xenopus* (Kofron et al., 2002). Since γ-catenin can also associate with CPI-17, an inhibitor of MLC phosphatase, this might contribute to the overall regulation of MLC phosphorylation at the junction (Kim et al., 2013) supporting broader effects of γ-catenin on junctional F-actin and on adherens junctions.

The identification of the EMMPRIN/γ-catenin complex raises the question of how it regulates actomyosin contractility and junction stability. ATP is required for phosphorylation of MLC by MLCK, and we therefore explored the possible role of Nm23, a member of the nucleoside diphosphate kinase (NDPK) family, which was recently identified as a partner of γ-catenin in tumor cells (Aktary et al., 2010). Nm23 could be found at endothelial junctions together with EMMPRIN and γ-catenin and interference of either of these proteins resulted in a significant decrease of Nm23 location at these sites. A myristoylated EMMPRIN cytosolic tail rescuedγ -catenin and Nm23 presence at junctions together with pMLC and F-actin organization at these sites further supporting an essential

contribution of the EMMPRIN/γ-catenin/Nm23 complex to the regulation of tension at junctions. A detailed analysis of how this molecular complex is assembled and the protein domains involved in the interactions deserves further investigation.

The mechanism by which Nm23 might regulate endothelial intercellular adhesion remained however unclear. The primary function of NDPK is to provide phosphates to ADP thus generating ATP which could then be used for myosin-dependent cytoskeleton contraction, as reported in *Dictyostelium* (Gajewski et al., 2003). By using by the first time in ECs the recently developed Perceval tool (Berg et al., 2009; Zala et al., 2013), we could visualize and quantitate ATP/ADP ratios at the subcellular level and show that in inhibitor-treated cells, the absence of EMMPRIN resulted in lower ATP/ADP ratios at the junctional area compared to control cells. The requirement for local ATP production of EMMPRIN at the endothelial membrane was further confirmed in isolated membranes; in addition, the ability of an inhibitory anti-Nm23 antibody to mimic the effect of EMMPRIN depletion, significantly reducing ATP production in membranes, further demonstrates the contribution of Nm23 to ATP production within the EMMPRIN/γ-catenin complex at human endothelial junctions. The EMMPRIN/γ-catenin/Nm23 complex would provide a local source of ATP required for MLCK-dependent MLC phosphorylation and actomyosin-driven forces at junctions; alternatively local ATP can be crucial for dynamic regulation of weak/strong actomyosin force cycles required for efficient contractility (Aprodu et al., 2008). This Nm23/NDPK function would be particularly important when ATP levels are low (Aguado-Velasco et al., 1996), as might be the case at maturing junctions, where the packed actin cytoskeleton might restrict free diffusion of ATP from the cytosol. Nm23 interference resulted however in a more severe junction phenotype than the one observed in EMMPRIN- or γ-catenin-interfered ECs since in addition to decreased junctional pMLC and increased linearity index and to altered VE-cadherin pattern and augmented monolayer permeability, ECs displayed lamellipodia-like at the cell-cell adhesions resembling disrupted junctions. This might be related to global cellular effects of Nm23 interference and to additional functions attributed to Nm23 in regulating adherens junctions such as Rab5-mediated endocytosis and inhibition of Rac signaling by sequestering Rac GEFs in *Drosophila,* and Arf6-dependent E-cadherin endocytosis in canine epithelial cells (Palacios et al., 2002; Woolworth et al., 2009). The EMMPRIN/γ-catenin/Nm23 complex identifies

an unexpected link between compartmentalized energy production and EC junction stability that might be relevant to situations in which changes in EC metabolism and junction remodeling need to be coordinated, such as angiogenesis, collective migration and tissue morphogenesis.

MATERIALS AND METHODS

Mice

EMMPRIN-deficient mice were generated as described previously (Muramatsu and Miyauchi, 2003). EMMPRIN heterozygotes were crossed following the strategy previously described (Chen et al., 2004) and null littermates were used for experiments. Mice were kept in the CNIC Animal Facility under pathogen-free conditions and according to institutional guidelines. All animal studies were approved by the CNIC Animal Care Ethical Committee.

Antibodies and reagents

Monoclonal mouse antibody VJ1/9.1 against EMMPRIN ectodomain was generated in Dr. Sanchez-Madrid's laboratory. Anti-VE-cadherin TEA1/31 and anti-PECAM-1 TP1/15 mAbs have been described previously (Yanez-Mo et al., 1998). Anti-JAM-A BV16 mAb was obtained from Hycult Biotech. Rabbit anti-phospho-myosin light chain (pMLC) antibody was from Cell Signaling, rabbit anti-myosin light chain from Santa Cruz, and phalloidin-Texas Red was obtained from BD Pharmingen. Whole mount mouse vessels were stained with anti-PECAM-1 from Millipore, anti-VE-cadherin and anti-γ-catenin from BD Biosciences, and anti-EMMPRIN from eBiosciences. Goat anti-mouse, anti-armenian hamster and anti-rat secondary antibodies were from Jackson ImmunoResearch. Collagen I was purchased from PureCol, OPTIMEM from Gibco, medium 199 from Lonza, Evans Blue from Sigma and Oligofectamine and dextran-TRITC from Invitrogen. The Rho kinase inhibitor Y27632 was obtained from Sigma. Anti-Nm23 antibodies were purchased from Santa Cruz Biotechnology and GeneTex. LifeAct (Riedl et al., 2008) and myristoylated cytosolic EMMPRIN (Ruiz et al., 2008) constructs were provided by Dr. Roland Wedlich-Soldner and Dr. Xosé Bustelo, respectively.

Whole mount staining

Mice were perfused with 1% PFA in PBS. Postnatal retinas and the trachea, aorta and ears of adult animals were extracted and post-fixed in 1% PFA for 1 h at room temperature (RT). Tissues were then incubated with primary antibodies in 5% goat serum (Jackson ImmunoResearch) overnight at room temperature (RT). Samples were then washed for 8 h in PBS-0.3% TX-100 and labeled with the appropriate secondary antibody overnight at RT. The next day, samples were washed again in PBS-0.3% TX-100 and mounted in

Vectashield (Vector Laboratories). Samples were examined with a Leica TCS Sp5 spectral confocal microscope or a Zeiss LSM 700 confocal microscope.

In vivo permeability assay

A modified Miles assay was used to examine vessel permeability in 4-8-week old anesthetized mice (Miles and Miles, 1952). Briefly, the mice were injected intravenously with 100 µl of 5 mg/ml of dextran-TRITC (4KDa or 70KDa) or 100 µl of 30 mg/kg Evans Blue, and after 5 min 5% mustard oil in mineral oil (Sigma) was applied to the right ear. Mineral oil alone was applied to the left ear as a negative control. After 30 min mice were sacrificed and ears from dextran-injected mice were extracted and processed for whole mount staining and ears from Blue Evans-injected mice were dried and weighted. For analysis of basal leakage in different organs, animals were sacrificed 18-20 h after injection. Evans Blue was extracted from tissues in formamide (Fluka) and measured in a spectrophotometer (BioRad).

Cell culture

Human umbilical vein endothelial cells (HUVEC) were obtained and cultured as described previously (Yanez-Mo et al., 1998). Cells from passages two to four were used in all assays. For endothelial monolayer formation assay, HUVEC were seeded at subconfluence on collagen I-coated plates or coverslips. Cells were processed for analysis 1, 24, 48, and 72 h after seeding. Mouse lung endothelial cells (MLEC) were obtained and cultured as described (Oblander et al., 2005). Briefly, lungs from WT or EMMPRIN-null mice were excised, disaggregated and digested in 0.1% collagenase (GIBCO) for 1 h at 37ºC. The cell suspensions were seeded onto plates coated with 10µg/ml fibronectin (Sigma), 10 µg/ml collagen I (PureCol) and 0.1% gelatin (Sigma). After attachment, cells were negatively selected with anti-CD16/CD32 mAb (BD Biosciences) coupled to magnetic beads (Dynal, Invitrogen), and then positively selected with anti-ICAM-2 (BD Biosciences) coupled to magnetic beads. Cells were seeded onto plates coated with 10µg/mL collagen I before assays.

Immunofluorescence microscopy

Tissue cryosections were fixed with 4% paraformaldehyde (PFA), 2% sucrose in PBS for 15 min and quenched for 1 h at RT with 100 mM glycine in PBS. After washing, sections were blocked overnight with 2% BSA and 5% goat serum in PBS. Sections were then

incubated with primary antibodies for 2-3 h at 37ºC. After washes, samples were incubated with goat secondary antibodies for 1 h at 37ºC, washed again and mounted with Prolong (Invitrogen). Cells were grown on collagen I-coated coverslips and samples fixed at different times in 4% PFA, 2% sucrose in PBS for 15 min at RT. Samples were blocked with 2% BSA and when necessary permeabilized with 0.1% Triton X100 for 10 min. For colocalization of Nm23 with EMMPRIN and γ-catenin cells were also fixed in methanol at -20ºC for 2 min or treated with saponin 0.01% for 5 min at RT before PFA fixation. Coverslips were incubated with the primary antibody for 1 h at 37º and, after washes, labeled with the appropriate secondary antibody under the same conditions. For double staining of EMMPRIN and other molecules using mouse antibodies, immunofluorescence was performed as described above and coverslips were incubated with anti-EMMPRIN (VJ1/9.1) directly labeled with Alexa488 or Alexa594 (Zenon, Molecular Probes).

Proximity ligation assay (PLA)

Human ECs were fixed with methanol at -20ºC for 2 min and stained with rabbit antibody anti-EMMPRIN C-terminus (GTX62657, Genetex) and mouse anti-γ-catenin or with mouse anti-γ-catenin and rabbit anti-Nm23. PLA was performed following provider's instructions (Duolink In Situ kit, Olink Biosciences). Briefly, samples were blocked with the blocking solution for 30 min at 37ºC and incubated overnight with the primary antibodies at 4ºC. Next day the samples were washed and incubated for 1 h at 37ºC with PLA probes for rabbit and mouse antibodies. After washing, samples were incubated with the ligase for 30 min at 37ºC, washed again and incubated with the polymerase for 100 min at 37ºC. Finally, the samples were washed, totally dried and mounted in Duolink In Situ Mounting Medium with DAPI.

siRNA interference and transfections

HUVEC ($3x10^5$) were seeded on collagen-I-coated p6 plates the day before siRNA transfection. The next morning, two independent EMMPRIN siRNA oligonucleotides or negative siRNA (Ambion) were mixed with 4 µl Oligofectamine (Invitrogen) in 400 µl Opti-MEM and added to the cells (final concentration 100 nM). After 4 h, 600 µl of OPTIMEM containing 30% FBS were added and the cells were incubated overnight at 37ºC. Most experiments were performed with both siRNAs, but for some experiments results are shown for siRNA#1 only, which decreases EMMPRIN expression less

efficiently than siRNA#2 but in a higher percentage of cells. Transfection of HUVEC with γ-catenin or Nm23 siRNA oligonucleotides (Ambion) followed a similar protocol. For expression of LifeAct or the myristoylated cytosolic tail of EMMPRIN, cells were first interfered as described and the next day were transfected with 2 μg DNA in Lipofectamine 2000 (Invitrogen). Cells were analyzed 24 h after transfection.

Time-lapse videomicroscopy experiments

After siRNA interference, HUVEC were transfected with LifeAct and seeded on ColI-coated glass-bottom plates. Before imaging, cells were stained with Zenon Alexa 488 (Molecular Probes)-directly labeled anti-EMMPRIN antibody (VJ1/9.1) for 30 min at RT. For time-lapse videomicroscopy, cells were kept at 37º C with 5% of CO_2 and Z-stacks of eight confocal sections (1,2 μM) were taken every 5 min with a Zeiss LSM 700 microscope for 20 h.

Image acquisition and analysis

Images were acquired with objectives 40x/1,25 or 63x/1,4 in a Sp5 confocal microscope (Leica Microsystems) or with objectives 40x/1,3 or 63x/1,4 in a LSM700 confocal microscope (Carl Zeiss). Images were converted to Tiff file with LAS AF (Leica Microsystems) or ZEN (Carl Zeiss) software, respectively and brightness and contrast were adjusted with Photoshop CS3. Colocalization of EMMPRIN with other junction proteins was analyzed with LAS AF software. Data are presented as the percentage of colocalization measured in regions of interest (ROIs) surrounding the junction. Junctional ROIs were drawn as an area with a maximum width of 1,5-2 μm surrounding the junction. The VE-cadherin fluorescence staining pattern was quantified with Image J making plot profiles within similar ROIs as in colocalization analysis. In each of three independent experiments, 4-6 junctions were analyzed per field in an average of 5 fields. Fluorescence intensities for γ-catenin, Nm23, pMLC and F-actin were also analyzed with Image J. Mean intensity per pixel was measured in junctional ROIs and in the rest of the cell (interior). Linearity index as defined by the ratio of junction length to the distance between vertices by Takeichi's group (Otani et al., 2006) was quantified by Image J software based on VE-cadherin staining of endothelial cell junction length.

In vitro permeability assay

HUVEC monolayer permeability was measured with the Millipore In Vitro Permeability Assay kit. Briefly, 120,000 cells were seeded on the membranes of the chambers provided with the kit. After 48h dextran-FITC was added to the upper chamber, and was recovered at different times from the bottom chamber and measured in a fluorimeter (Fluoroskan Ascent, Thermo Scientific).

Tugging forces

PDMS microneedle array substrates were fabricated as in (Fu et al., 2010). Bowtie patterns had a total area of 1600 μm^2. To measure forces exerted at the junctions, control HUVEC (Neg) or EMMPRIN-interfered cells (siRNA#1 and siRNA#2) were plated over elastomer sensors with fibronectin micropatterning and fixed with 4% PFA in PBS for 15 min and stained for EMMPRIN. Tugging forces were measured as described (Liu et al., 2010). Briefly, microneedle deflections were calculated using Matlab to determine the displacement of the centroid of the microneedle at the tip. Forces were then computed from the known spring constant of the microneedle (7.2 nN/μm). Cells exist in a quasi-static equilibrium where the net force sums to zero (Balaban et al., 2001; Tan et al., 2003). The intercellular tugging force is therefore equal in magnitude and opposite in direction to the measured net traction force reported by the microneedle array (Cohen et al., 2013; Liu et al., 2010).

Coimmunoprecipitation and western blot

Cells were lysed in RIPA buffer for 5 min at 4º C and scraped. Lysates were cleared by spinning at 15000 rpm, 4ºC for 15 min, and 5x Laemmli buffer was added to the supernatant. Cell proteins were resolved by SDS-PAGE and transferred to nitrocellulose membranes. Blots were blocked overnight at 4ºC in TBS-T containing 5% BSA and incubated with primary and secondary antibodies in TBS-T for 1 h at RT. Signal on washed blots was detected by enhanced chemiluminescence (GE Healthcare Life Sciences). For pMLC and MLC detection, membranes from control- and EMMPRIN-interfered human ECs were isolated as detailed in ATP production assays below and blots processed as just described. For coimmunoprecipitation, confluent cells were incubated for 1 h at 4ºC with VJ1/9.1 mAb or an IgG1 control (2μg each per $3x10^6$ cells). Cells were lysed and cleared as before, and the lysates were incubated with protein G-Sepharose (GE Healthcare Life

Sciences) for 1 h at 4ºC. Beads were washed six times with lysis buffer and the proteins were separated and immunodetected as above.

Perceval assay

After siRNA interference, HUVEC were transfected with Perceval plasmid (Addgene) by the calcium phosphate method (Armesilla et al., 1999) and analyzed in a Zeiss LSM 700 confocal microscope equipped with a x40 oil-immersion objective. For Perceval signal, excitation was set at 405 nm (ADP sensitive) and 488 nm (ATP sensitive) and detection of PMT was set at 500–560 nm. Thirty minutes before the experiment, human ECs were stained with the directly labeled (Zenon)-anti-EMMPRIN antibody to identify EMMPRIN-interfered cells. As a control for possible effects of pH variations on ATP/ADP signal, pH was registered by adding 5 µM SNARF 5 probe (Life Technologies) in complete medium for 25 min, 1 h before the experiment. For SNARF 5, excitation was set at 555 nm and detection of PMT was set at 575–595 nm (pH sensitive) and 610–647 nm (pH insensitive). pH and Perceval (ATP/ADP) signals were quantified by the ratio intensity of the two corresponding detection channels. To inhibit ATP production by mitochondria and glycolysis, human ECs were treated with rotenone (1 µM), oligomycin (5 µM) and 2-deoxyglucose (20 mM) (all from Sigma-Aldrich). Cells were visualized and ATP/ADP ratios quantified in a time-range before and after treatment with the combination of inhibitors in which no variations of pH were observed. Analysis of the intensity ratios was done with Image J in the cell periphery (equivalent to junctional ROI) and in the total cellular area.

Membrane fractioning and ATP production assay

Cells were washed and treated with ice-cold hypotonic lysis buffer (10 mM Tris-HCl at pH 7.4, 1.5 mM $MgCl_2$, 5 mM KCl, 1 mM dithiothreitol, 0.2 mM sodium vanadate, and protease inhibitors) for 5 min. Cell lysates were homogenized with 30 strokes of a Dounce homogenizer and homogenates were centrifuged at 1000 g for 3 min. The supernatants were then spun at 40,000 g for 30 min at 4°C in a refrigerated centrifuge and the crude membrane pellet was gently washed with hypotonic lysis buffer and resuspended in RIPA buffer. Membrane fractions were then assayed for total protein. ATP production by membrane-enriched fractions was measured by a kinetic luminescence assay (Vives-Bauza et al., 2007). Briefly, enriched membranes were diluted in buffer A (150 mM KCl, 25 mM

Tris-HCl, 2 mM EDTA, 0.1% BSA, 10 mM KPO_4, 0.1 mM $MgCl_2$, pH 7.4) in the presence of 150 μM ADP**,** 150 μM GTP, 1 μM oligomycin and 150 μM diadenosin pentaphosphate. To inhibit the reaction, anti-Nm23 antibody (Santa Cruz biotechnology) was added at a final dilution of 1:100.

Statistical analysis

Student's t test was used for statistical comparisons of two groups of data. For three or more groups assuming Gaussian distribution, one-way ANOVA with Dunnet's multiple comparisons post-test was used for comparisons with controls, and Newman-Keuls test was used for comparisons between different groups of data.

Acknowledgments

We thank Dr. Roland Wedlich-Soldner for LifeAct and Dr. Xosé Bustelo for myr-EMMPRIN cytosolic constructs, respectively, and S. Bartlett for English editing. This work was supported by grants from Fundación Ramón Areces and Ministerio de Economía y Competitividad RD12/0042/0023 and SAF2011-25619 to AGA, grants RD12/0042/0056 and ERC-2011AdG 294340 GENTRIS to FS-M, grants from the Associazione Italiana per la Ricerca sul Cancro and European Research Council to ED, and grants from NIH, the RESBIO Technology Resource for Polymeric Biomaterials, and the Penn Nano/Bio Interface Center to CC. VM was funded by the Comunidad Autónoma de Madrid (S2010/BMD-2312 Angiobodies 2.0). The CNIC is supported by the Ministerio de Economía y Competitividad and the Pro-CNIC Foundation.

Author contributions: V.M. designed experiments, performed research and wrote the paper; P.G., J.G-E., A.P. and R.A-P. performed research; M.Y-M. performed proteomics analysis; O.B. and K.K. contributed reagents and analytical tools; F.O. contributed experimental techniques; M.B. and C.C. performed elastomer sensor experiments; J.A.E., E.D. and F.S.M. contributed techniques or reagents and discussion; and A.G.A. designed the research and wrote the paper.

The authors declare no conflict of interest.

REFERENCES

Abraham, S., Yeo, M., Montero-Balaguer, M., Paterson, H., Dejana, E., Marshall, C. J. and Mavria, G. (2009). VE-Cadherin-mediated cell-cell interaction suppresses sprouting via signaling to MLC2 phosphorylation. *Curr Biol* **19**, 668-74.

Aguado-Velasco, C., Veron, M., Rambow, J. A. and Kuczmarski, E. R. (1996). NDP kinase can modulate contraction of Dictyostelium cytoskeletons. *Cell Motil Cytoskeleton* **34**, 194-205.

Aktary, Z., Chapman, K., Lam, L., Lo, A., Ji, C., Graham, K., Cook, L., Li, L., Mackey, J. R. and Pasdar, M. (2010). Plakoglobin interacts with and increases the protein levels of metastasis suppressor Nm23-H2 and regulates the expression of Nm23-H1. *Oncogene* **29**, 2118-29.

Ando, K., Fukuhara, S., Moriya, T., Obara, Y., Nakahata, N. and Mochizuki, N. (2013). Rap1 potentiates endothelial cell junctions by spatially controlling myosin II activity and actin organization. *J Cell Biol* **202**, 901-16.

Aprodu, I., Redaelli, A. and Soncini, M. (2008). Actomyosin interaction: mechanical and energetic properties in different nucleotide binding states. *Int J Mol Sci* **9**, 1927-43.

Armesilla, A. L., Lorenzo, E., Gomez del Arco, P., Martinez-Martinez, S., Alfranca, A. and Redondo, J. M. (1999). Vascular endothelial growth factor activates nuclear factor of activated T cells in human endothelial cells: a role for tissue factor gene expression. *Mol Cell Biol* **19**, 2032-43.

Balaban, N. Q., Schwarz, U. S., Riveline, D., Goichberg, P., Tzur, G., Sabanay, I., Mahalu, D., Safran, S., Bershadsky, A., Addadi, L. et al. (2001). Force and focal adhesion assembly: a close relationship studied using elastic micropatterned substrates. *Nat Cell Biol* **3**, 466-72.

Baum, B. and Georgiou, M. (2011). Dynamics of adherens junctions in epithelial establishment, maintenance, and remodeling. *J Cell Biol* **192**, 907-17.

Berditchevski, F., Chang, S., Bodorova, J. and Hemler, M. E. (1997). Generation of monoclonal antibodies to integrin-associated proteins. Evidence that alpha3beta1 complexes with EMMPRIN/basigin/OX47/M6. *J Biol Chem* **272**, 29174-80.

Berg, J., Hung, Y. P. and Yellen, G. (2009). A genetically encoded fluorescent reporter of ATP:ADP ratio. *Nat Methods* **6**, 161-6.

Besse, F., Mertel, S., Kittel, R. J., Wichmann, C., Rasse, T. M., Sigrist, S. J. and Ephrussi, A. (2007). The Ig cell adhesion molecule Basigin controls compartmentalization and vesicle release at Drosophila melanogaster synapses. *J Cell Biol* **177**, 843-55.

Bougatef, F., Quemener, C., Kellouche, S., Naimi, B., Podgorniak, M. P., Millot, G., Gabison, E. E., Calvo, F., Dosquet, C., Lebbe, C. et al. (2009). EMMPRIN promotes angiogenesis through hypoxia-inducible factor-2alpha-mediated regulation of soluble VEGF isoforms and their receptor VEGFR-2. *Blood* **114**, 5547-56.

Cohen, D. M., Yang, M. T. and Chen, C. S. (2013). Measuring Cell-Cell Tugging Forces Using Bowtie-Patterned mPADs (Microarray Post Detectors). *Methods Mol Biol* **1066**, 157-68.

Conway, D. E., Breckenridge, M. T., Hinde, E., Gratton, E., Chen, C. S. and Schwartz, M. A. (2013). Fluid shear stress on endothelial cells modulates mechanical tension across VE-cadherin and PECAM-1. *Curr Biol* **23**, 1024-30.

Chen, S., Kadomatsu, K., Kondo, M., Toyama, Y., Toshimori, K., Ueno, S., Miyake, Y. and Muramatsu, T. (2004). Effects of flanking genes on the phenotypes of mice deficient in basigin/CD147. *Biochem Biophys Res Commun* **324**, 147-53.

Chen, Y., Zhang, H., Gou, X., Horikawa, Y., Xing, J. and Chen, Z. (2009). Upregulation of HAb18G/CD147 in activated human umbilical vein endothelial cells enhances the angiogenesis. *Cancer Lett* **278**, 113-21.

Dejana, E. (2004). Endothelial cell-cell junctions: happy together. *Nat Rev Mol Cell Biol* **5**, 261-70.

Dejana, E., Tournier-Lasserve, E. and Weinstein, B. M. (2009). The control of vascular integrity by endothelial cell junctions: molecular basis and pathological implications. *Dev Cell* **16**, 209-21.

Deora, A. A., Gravotta, D., Kreitzer, G., Hu, J., Bok, D. and Rodriguez-Boulan, E. (2004). The basolateral targeting signal of CD147 (EMMPRIN) consists of a single leucine and is not recognized by retinal pigment epithelium. *Mol Biol Cell* **15**, 4148-65.

Deora, A. A., Philp, N., Hu, J., Bok, D. and Rodriguez-Boulan, E. (2005). Mechanisms regulating tissue-specific polarity of monocarboxylate transporters and their chaperone CD147 in kidney and retinal epithelia. *Proc Natl Acad Sci U S A* **102**, 16245-50.

Fu, J., Wang, Y. K., Yang, M. T., Desai, R. A., Yu, X., Liu, Z. and Chen, C. S. (2010). Mechanical regulation of cell function with geometrically modulated elastomeric substrates. *Nat Methods* **7**, 733-6.

Gajewski, C. D., Yang, L., Schon, E. A. and Manfredi, G. (2003). New insights into the bioenergetics of mitochondrial disorders using intracellular ATP reporters. *Mol Biol Cell* **14**, 3628-35.

Giannotta, M., Trani, M. and Dejana, E. (2013). VE-Cadherin and Endothelial Adherens Junctions: Active Guardians of Vascular Integrity. *Dev Cell* **26**, 441-54.

Graesser, D., Solowiej, A., Bruckner, M., Osterweil, E., Juedes, A., Davis, S., Ruddle, N. H., Engelhardt, B. and Madri, J. A. (2002). Altered vascular permeability and early onset of experimental autoimmune encephalomyelitis in PECAM-1-deficient mice. *J Clin Invest* **109**, 383-92.

Hoelzle, M. K. and Svitkina, T. (2012). The cytoskeletal mechanisms of cell-cell junction formation in endothelial cells. *Mol Biol Cell* **23**, 310-23.

Huveneers, S., Oldenburg, J., Spanjaard, E., van der Krogt, G., Grigoriev, I., Akhmanova, A., Rehmann, H. and de Rooij, J. (2012). Vinculin associates with endothelial VE-cadherin junctions to control force-dependent remodeling. *J Cell Biol* **196**, 641-52.

Kim, K. M., Adyshev, D. M., Kasa, A., Zemskov, E. A., Kolosova, I. A., Csortos, C. and Verin, A. D. (2013). Putative protein partners for the human CPI-17 protein revealed by bacterial two-hybrid screening. *Microvasc Res* **88**, 19-24.

Kofron, M., Heasman, J., Lang, S. A. and Wylie, C. C. (2002). Plakoglobin is required for maintenance of the cortical actin skeleton in early Xenopus embryos and for cdc42-mediated wound healing. *J Cell Biol* **158**, 695-708.

Liu, Z., Tan, J. L., Cohen, D. M., Yang, M. T., Sniadecki, N. J., Ruiz, S. A., Nelson, C. M. and Chen, C. S. (2010). Mechanical tugging force regulates the size of cell-cell junctions. *Proc Natl Acad Sci U S A* **107**, 9944-9.

Maldonado-Baez, L., Cole, N. B., Kramer, H. and Donaldson, J. G. (2013). Microtubule-dependent endosomal sorting of clathrin-independent cargo by Hook1. *J Cell Biol* **201**, 233-47.

Mege, R. M., Gavard, J. and Lambert, M. (2006). Regulation of cell-cell junctions by the cytoskeleton. *Curr Opin Cell Biol* **18**, 541-8.

Miles, A. A. and Miles, E. M. (1952). Vascular reactions to histamine, histamine-liberator and leukotaxine in the skin of guinea-pigs. *J Physiol* **118**, 228-57.

Millimaggi, D., Mari, M., D'Ascenzo, S., Carosa, E., Jannini, E. A., Zucker, S., Carta, G., Pavan, A. and Dolo, V. (2007). Tumor vesicle-associated CD147 modulates the angiogenic capability of endothelial cells. *Neoplasia* **9**, 349-57.

Muramatsu, T. and Miyauchi, T. (2003). Basigin (CD147): a multifunctional transmembrane protein involved in reproduction, neural function, inflammation and tumor invasion. *Histol Histopathol* **18**, 981-7.

Oblander, S. A., Zhou, Z., Galvez, B. G., Starcher, B., Shannon, J. M., Durbeej, M., Arroyo, A. G., Tryggvason, K. and Apte, S. S. (2005). Distinctive functions of membrane type 1 matrix-metalloprotease (MT1-MMP or MMP-14) in lung and submandibular gland development are independent of its role in pro-MMP-2 activation. *Dev Biol* **277**, 255-69.

Orlova, V. V., Economopoulou, M., Lupu, F., Santoso, S. and Chavakis, T. (2006). Junctional adhesion molecule-C regulates vascular endothelial permeability by modulating VE-cadherin-mediated cell-cell contacts. *J Exp Med* **203**, 2703-14.

Otani, T., Ichii, T., Aono, S. and Takeichi, M. (2006). Cdc42 GEF Tuba regulates the junctional configuration of simple epithelial cells. *J Cell Biol* **175**, 135-46.

Palacios, F., Schweitzer, J. K., Boshans, R. L. and D'Souza-Schorey, C. (2002). ARF6-GTP recruits Nm23-H1 to facilitate dynamin-mediated endocytosis during adherens junctions disassembly. *Nat Cell Biol* **4**, 929-36.

Prasain, N. and Stevens, T. (2009). The actin cytoskeleton in endothelial cell phenotypes. *Microvasc Res* **77**, 53-63.

Riedl, J., Crevenna, A. H., Kessenbrock, K., Yu, J. H., Neukirchen, D., Bista, M., Bradke, F., Jenne, D., Holak, T. A., Werb, Z. et al. (2008). Lifeact: a versatile marker to visualize F-actin. *Nat Methods* **5**, 605-7.

Ruiz, S., Castro-Castro, A. and Bustelo, X. R. (2008). CD147 inhibits the nuclear factor of activated T-cells by impairing Vav1 and Rac1 downstream signaling. *J Biol Chem* **283**, 5554-66.

Schreiner, A., Ruonala, M., Jakob, V., Suthaus, J., Boles, E., Wouters, F. and Starzinski-Powitz, A. (2007). Junction protein shrew-1 influences cell invasion and interacts with invasion-promoting protein CD147. *Mol Biol Cell* **18**, 1272-81.

Smutny, M., Cox, H. L., Leerberg, J. M., Kovacs, E. M., Conti, M. A., Ferguson, C., Hamilton, N. A., Parton, R. G., Adelstein, R. S. and Yap, A. S. (2010). Myosin II isoforms identify distinct functional modules that support integrity of the epithelial zonula adherens. *Nat Cell Biol* **12**, 696-702.

Tan, J. L., Tien, J., Pirone, D. M., Gray, D. S., Bhadriraju, K. and Chen, C. S. (2003). Cells lying on a bed of microneedles: an approach to isolate mechanical force. *Proc Natl Acad Sci U S A* **100**, 1484-9.

Tang, W. and Hemler, M. E. (2004). Caveolin-1 regulates matrix metalloproteinases-1 induction and CD147/EMMPRIN cell surface clustering. *J Biol Chem* **279**, 11112-8.

Totsukawa, G., Yamakita, Y., Yamashiro, S., Hartshorne, D. J., Sasaki, Y. and Matsumura, F. (2000). Distinct roles of ROCK (Rho-kinase) and MLCK in spatial

regulation of MLC phosphorylation for assembly of stress fibers and focal adhesions in 3T3 fibroblasts. *J Cell Biol* **150**, 797-806.

Vives-Bauza, C., Yang, L. and Manfredi, G. (2007). Assay of mitochondrial ATP synthesis in animal cells and tissues. *Methods Cell Biol* **80**, 155-71.

Wimmer, R., Cseh, B., Maier, B., Scherrer, K. and Baccarini, M. (2012). Angiogenic sprouting requires the fine tuning of endothelial cell cohesion by the Raf-1/Rok-alpha complex. *Dev Cell* **22**, 158-71.

Woolworth, J. A., Nallamothu, G. and Hsu, T. (2009). The Drosophila metastasis suppressor gene Nm23 homolog, awd, regulates epithelial integrity during oogenesis. *Mol Cell Biol* **29**, 4679-90.

Xu, D. and Hemler, M. E. (2005). Metabolic activation-related CD147-CD98 complex. *Mol Cell Proteomics* **4**, 1061-71.

Yanez-Mo, M., Alfranca, A., Cabanas, C., Marazuela, M., Tejedor, R., Ursa, M. A., Ashman, L. K., de Landazuri, M. O. and Sanchez-Madrid, F. (1998). Regulation of endothelial cell motility by complexes of tetraspan molecules CD81/TAPA-1 and CD151/PETA-3 with alpha3 beta1 integrin localized at endothelial lateral junctions. *J Cell Biol* **141**, 791-804.

Zala, D., Hinckelmann, M. V., Yu, H., Lyra da Cunha, M. M., Liot, G., Cordelieres, F. P., Marco, S. and Saudou, F. (2013). Vesicular glycolysis provides on-board energy for fast axonal transport. *Cell* **152**, 479-91.

FIGURE LEGENDS

Fig. 1. EMMPRIN-deficient mice show altered endothelial junctions and increased microvascular permeability. (A) Representative images of whole-mount staining in wild-type (EMMP+/+) and EMMPRIN null (EMMP-/-) mice for the junction marker PECAM-1 (green) in the trachea, ear and aorta. (B) The chart shows the quantification of Evans Blue tissue content in mustard-oil-inflamed and mineral-oil-control ears from wild-type and EMMPRIN-deficient mice. Data are means ± SEM of 4 independent experiments in a total of 16 mice per genotype (*** P <0.0001, unpaired t test). (C) Representative merged images of PECAM-1 staining (green) in the microvasculature of control and mustard-oil-inflamed ears of wild-type and EMMPRIN null mice 30 min after intravenous injection of 4kDa or 70kDa dextran-TRITC (red). Quantification of red fluorescence intensity is shown.

Fig. 2. VE-cadherin junctions are impaired in human and mouse EMMPRIN-deficient endothelial cell. (A) Representative western blot of EMMPRIN protein levels in HUVEC transfected with control siRNA (Neg) or EMMPRIN siRNAs up to 106 h post-transfection (equivalent to 72 h after seeding for monolayer formation). The chart on the right shows the efficiency of EMMPRIN silencing (% of protein expression compared to Neg siRNA at each time point). Tubulin is shown as loading control. (B) Representative images shown in B&W of immunostaining for VE-cadherin (red) and EMMPRIN (green) in HUVEC transfected with negative siRNA (Neg) or EMMPRIN siRNAs (#1 or #2). Control (Cn) indicates non-transfected HUVEC. Insets show magnified views of the boxed areas with detail of the VE-cadherin staining pattern at junctions. (C) Representative image analysis profiles of VE-cadherin staining performed as in A. The chart shows means ± SEM of the breadth of VE-cadherin staining at junctions; n=35 junctions quantified from 3 independent experiments per condition (***P<0.0001). (D) EMMPRIN knockdown increases endothelial monolayer permeability in vitro. HUVEC transfected as indicated were grown to confluence on transwell filters and dextran-FITC added to the upper chamber. Data are the means ± SEM of the amount of labeled dextran recovered in the lower chamber after 1 h (n=3; ** P=0.0023). (E) Representative images in B&W of staining for VE-cadherin in MLEC from wild-type and EMMPRIN null mice. Magnified views of the boxed areas are shown in the bottom.

Fig. 3. EMMPRIN is required for actin organization at endothelial junctions. (A) Representative images shown in B&W of staining for EMMPRIN (green), F-actin (phalloidin; red) and VE-cadherin (blue) in HUVEC 1 h and 48 h after seeding. Insets (right) show colocalization of EMMPRIN with F-actin at early and mature endothelial cell-cell contacts. (B) Representative images in B&W of staining for EMMPRIN (green) and F-actin (red) in control and EMMPRIN-interfered HUVEC 1 h after seeding. The boxed areas are shown in the magnified views; note the presence of a complex branched network of F-actin in control cells in contrast to perpendicular-to-the-junction F-actin filaments in EMMPRIN-interfered cells (particularly bottom right cell). (C) EMMPRIN-interfered HUVEC were transfected with LifeAct (red) and stained with directly labeled anti-EMMPRIN mAb (green). Starting 6 h after seeding, time-lapse images were recorded over 18 h. Selected images at the indicated time points are shown with cell numbers and dotted lines at the junctions depicted in white (for non-interfered cells) or yellow (for EMMPRIN-interfered cells).

Fig. 4. EMMPRIN regulates actomyosin contractility and tugging forces at endothelial junctions. (A) Representative images are shown in B&W of VE-cadherin, EMMPRIN, pMLC and F-actin staining in control and EMMPRIN-interfered HUVEC. Boxed regions are shown in the magnified views below the images. (B) Junctional regions of interest (ROIs) were drawn as an area with a maximum width of 1,5-2 μm surrounding the junction (identified by VE-cadherin staining). (C) Histograms show quantification of mean fluorescence intensity (MFI) for pMLC and F-actin at junctions of control and EMMPRIN-interfered HUVEC; n=30-40 junctions were quantified in 2-3 independent experiments per condition (**P<0.01, ***P<0.001). (D) Representative western blot of pMLC and MLC protein levels in enriched-membrane fractions isolated from Neg siRNA- and EMMPRIN-interfered human ECs (left); histogram shows fold induction (FI) of pMLC/MLC ratios in EMMPRIN-interfered versus control cells in n=3 independent experiments (right) (**P<0.01). (E) Similar images and image analysis as in A performed in aortas of wild-type and EMMPRIN null mice, showing junction staining with PECAM-1 (green) and pMLC (red), and F-actin (white) staining (left). 3D reconstruction from previous images of

endothelial junctions from wild-type or EMMPRIN-deficient aortas was performed with Imaris software (top, right). Volumes were partially transparent to allow visualization of all the components of the junction. (F) Histograms show the quantification of mean fluorescence intensity (MFI) for pMLC (green) and F-actin (phalloidin; red) at junctions of wild-type and EMMPRIN-deficient aortas; n=30-40 junctions were quantified from 2-3 independent experiments per condition (*P<0.05, ***P<0.001). (G) Linearity index was quantitated with Image J software as the ratio of the length of VE-cadherin junction staining and the distance between junction vertices in control, Neg siRNA- and EMMPRIN-interfered human ECs; n=40-50 junctions were quantified per condition in 3 independent experiments (***P<0.0001). (H) Tugging forces were quantified in EMMPRIN siRNA-transfected HUVEC plated on elastomer plates coated with fibronectin (red) and immunostained for EMMPRIN (green). Representative images with the force vectors (yellow) are shown on the left and on the right the graph showing the average of tugging forces for each condition ± SEM; n = 14, 8, 14 for negative siRNA, siRNA#1, and siRNA#2.

Fig. 5. EMMPRIN interacts with γ-catenin at endothelial cell junctions. (A) Representative western blot analysis for γ-catenin and VE-cadherin in EMMPRIN immunoprecipitates from HUVEC (left). Representative images in B&W are shown of immunofluorescence staining for EMMPRIN (red) and γ-catenin (green) in VE-cadherin-null mouse endothelial cells; insets show detail of the staining pattern at junctions (right). (B) Representative confocal fluorescence images of EMMPRIN (green), F-actin (phalloidin; red) and γ-catenin (blue) in HUVEC, showing colocalization of EMMPRIN and γ-catenin at 1 h and 48 h after seeding. (C) Representative confocal immunofluorescence images in B&W of staining of EMMPRIN (green) and γ-catenin (red) in control and EMMPRIN-interfered HUVEC at 48 h after seeding. (D) Representative western blot of γ-catenin protein levels in RIPA lysates from Neg siRNA- and EMMPRIN- interfered cells (left); histogram shows fold induction (FI) of γ-catenin amount in EMMPRIN-interfered versus control cells in n=3 independent experiments (right). (E) Representative images showing whole-mount staining of PECAM-1 (green) and γ-catenin (red) in the ears of wild-type and EMMPRIN null mice. (F) Representative images in B&W

are shown of staining for γ-catenin (blue), pMLC (green) and F-actin (phalloidin; red) in control and γ-catenin-interfered HUVEC. (G) Histograms show quantification of mean fluorescence intensities (MFI) for pMLC and F-actin at junctions of control versus γ-catenin-interfered HUVEC; n=30-40 junctions were quantified in 2-3 independent experiments per condition (*P<0.05, **P<0.01).

Fig. 6. Nm23 is associated with the EMMPRIN/γ-catenin complex at endothelial junctions. (A) Representative western blot analysis for Nm23 in EMMPRIN immunoprecipitates from HUVEC (left). (B) Top, representative confocal fluorescence images shown in B&W of staining of EMMPRIN (blue), γ-catenin (red) and Nm23 (green) in HUVEC at 48 h after seeding. Magnified views of the boxed areas are shown on the lower panels. Bottom, representative bright field and merged images of DAPI (blue) and proximity ligation assay (PLA, green) for EMMPRIN/γ-catenin (left) and for γ-catenin/ Nm23 (right) in HUVEC fixed with methanol. (C) Representative confocal fluorescence images shown in B&W of EMMPRIN (red) and Nm23 (green) in control and EMMPRIN-interfered HUVEC at 48 h after seeding (top). Histogram shows the quantification of mean fluorescence intensity (MFI) for Nm23 (green) at the junctions of control and EMMPRIN-interfered HUVEC (bottom); n=30-40 junctions were quantified in 3 independent experiments per condition (***P<0.001). (D) Representative confocal images shown in B&W of the staining of γ-catenin (red) and Nm23 (green) in non-interfered and γ-catenin siRNA-interfered HUVEC (top). Histogram shows the quantification of mean fluorescence intensity (MFI) for Nm23 (green) at the junctions of control and γ-catenin-interfered HUVEC (bottom); n=30-40 junctions were quantified in 2 independent experiments per condition (**P<0.01).

Fig 7. EMMPRIN cytosolic tail mediates γ-catenin and Nm23 recruitment and actomyosin contractility at endothelial junctions. Representative images are shown of EMMPRIN (red), γ-catenin (green) or Nm23 (green) (A) and of EMMPRIN (red), pMLC (green) or F-actin (phalloidin; green) (B) in EMMPRIN siRNA-interfered HUVEC transfected with a GFP myristoylated EMMPRIN cytosolic tail construct (blue). Histograms on the right show the quantification of mean fluorescence intensity (MFI) for γ-

catenin and Nm23 (A) or pMLC and F-actin (B) at the junctions of cells interfered for EMMPRIN and transfected or not with the GFP-myr EMMPRIN cytosolic tail. 30-50 junctions were analyzed in 2 independent experiments per group.

Fig. 8. **Nm23 presence at endothelial junctions is required for MLC phosphorylation and ATP production at these sites.** (A) Representative images in B&W of staining for Nm23 (blue), pMLC (green) and F-actin (phalloidin; red) and the merged images are shown in control and Nm23-interfered HUVEC. Boxed regions are shown in the magnified views below the images; dotted lines mark the junction in Nm23-interfered cells. (B) Histograms show quantification of mean fluorescence intensities (MFI) for pMLC and F-actin at junctions of control versus Nm23-interfered HUVEC; n=15 junctions were quantified in 2 independent experiments per condition (***P<0.001). (C) Histogram shows quantification of VE-cadherin linearity index in control versus Nm23-interfered HUVEC; n=20-30 junctions were quantified per condition in 2 independent experiments (***P<0.0001). (D) Representative images of human ECs stained for EMMPRIN and visualized for Perceval fluorescent signal (ATP/ADP ratio in pseudo-color scale) in the absence or presence of metabolic inhibitors in Neg- and EMMPRIN-interfered ECs (left). ATP/ADP ratios (average ± SEM.) quantified in the cell periphery (junctional area) are plotted in the range time in which pH was stable (around 3 min before and after addition of inhibitors) (middle). Histogram shows the relative drop in ATP/ADP ratio after inhibitor treatment normalizing basal levels to 1; n=6 cells analyzed for each condition. (E) ATP production in cell membranes from control and EMMPRIN-interfered HUVEC (n=3). Histograms show ATP generated by enzymatic reaction after addition of reaction buffer in the absence or presence of the inhibitory antibody anti-Nm23; Nm23-dependent ATP was calculated from the difference in ATP levels produced in the presence or absence of the antibody (*P<0.05, **P<0.01).

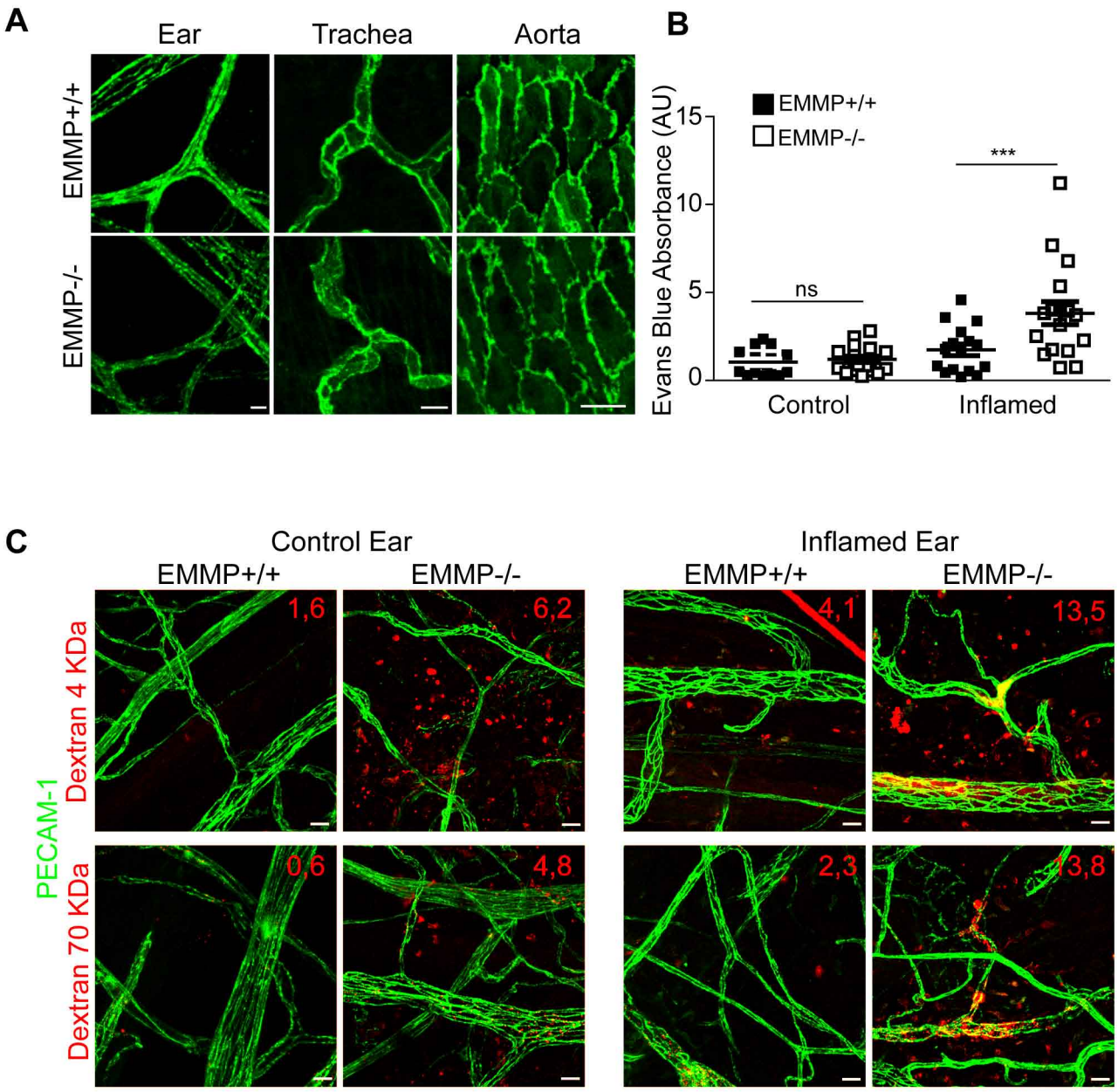

Figure 1

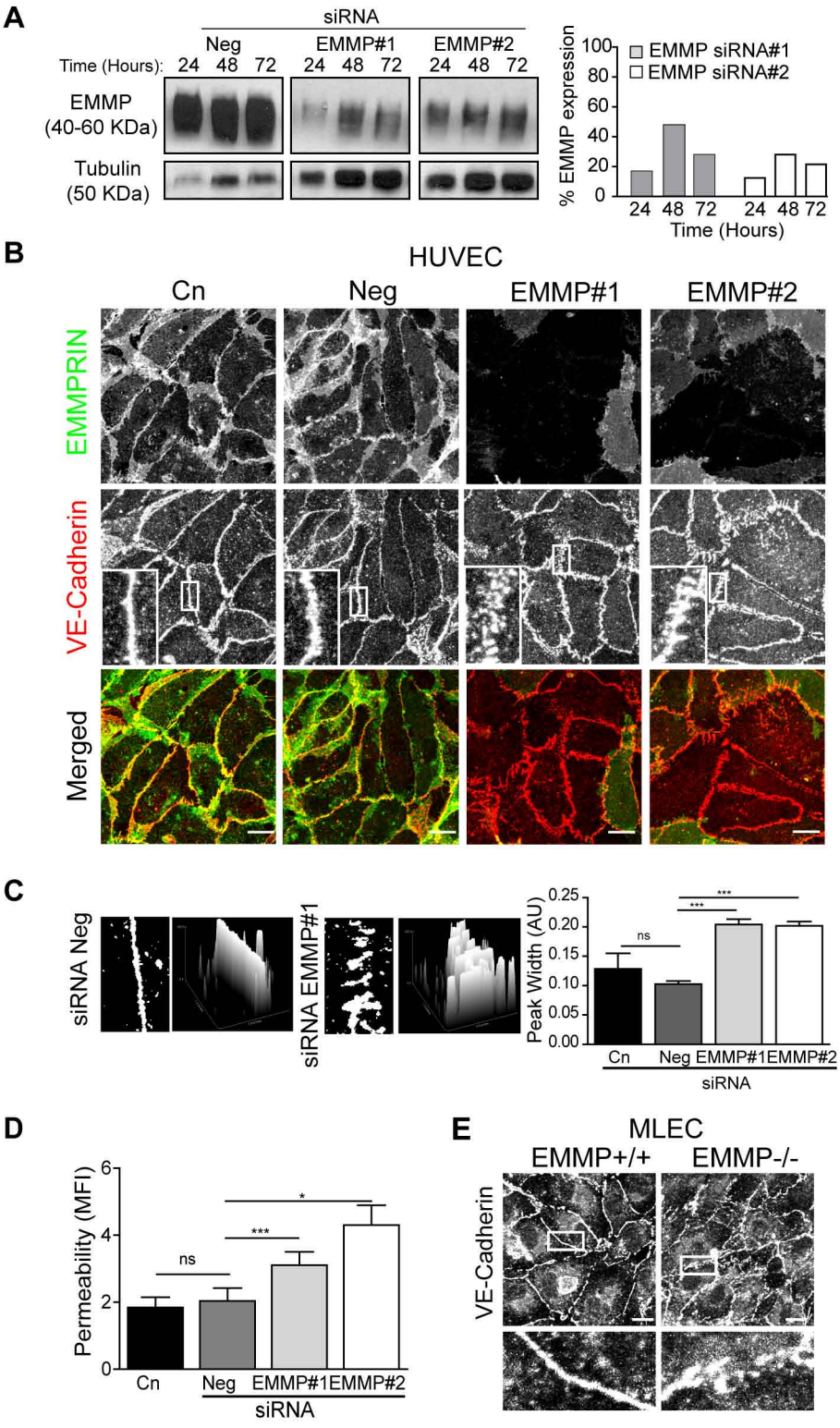

Figure 2

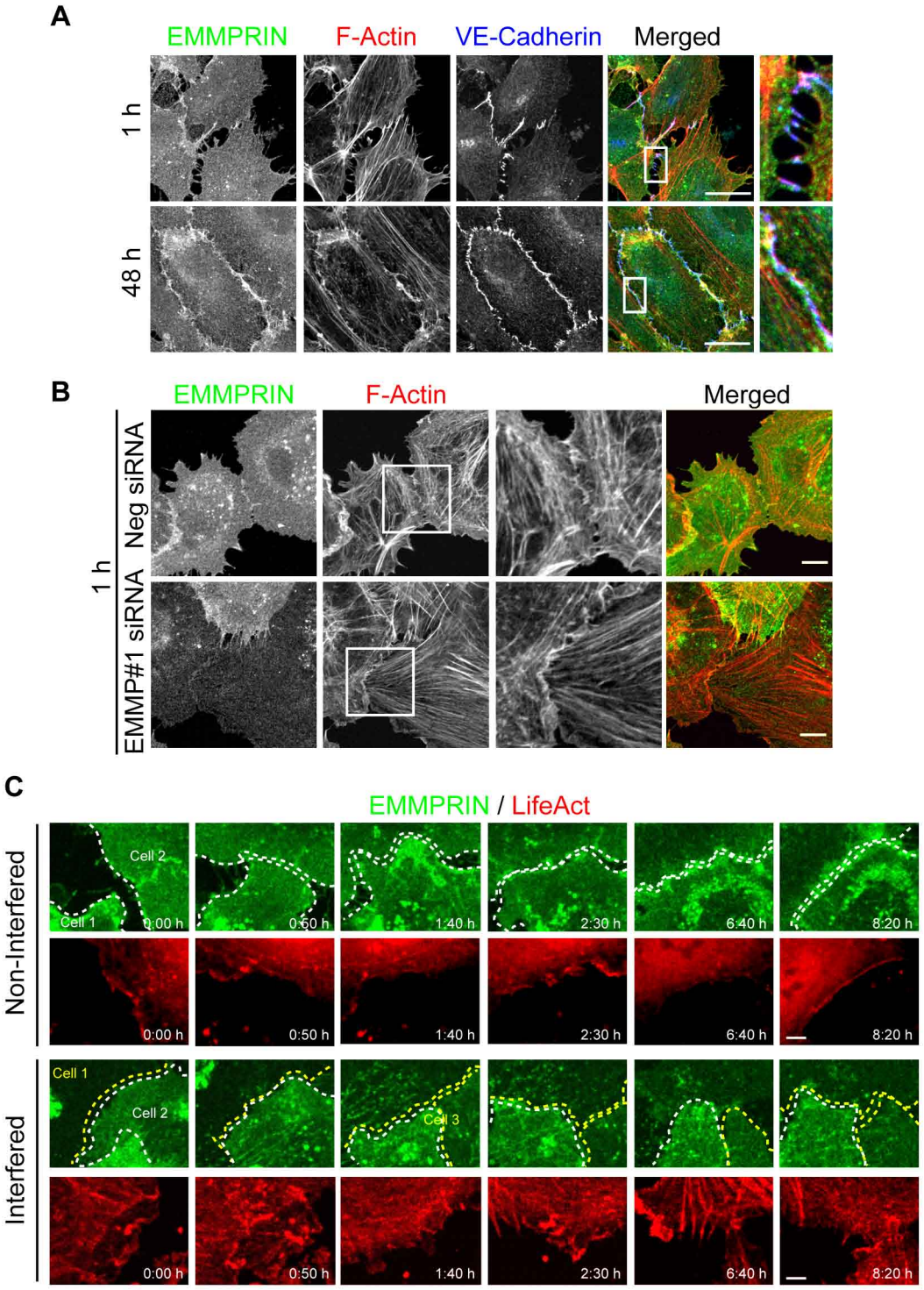

Figure 3

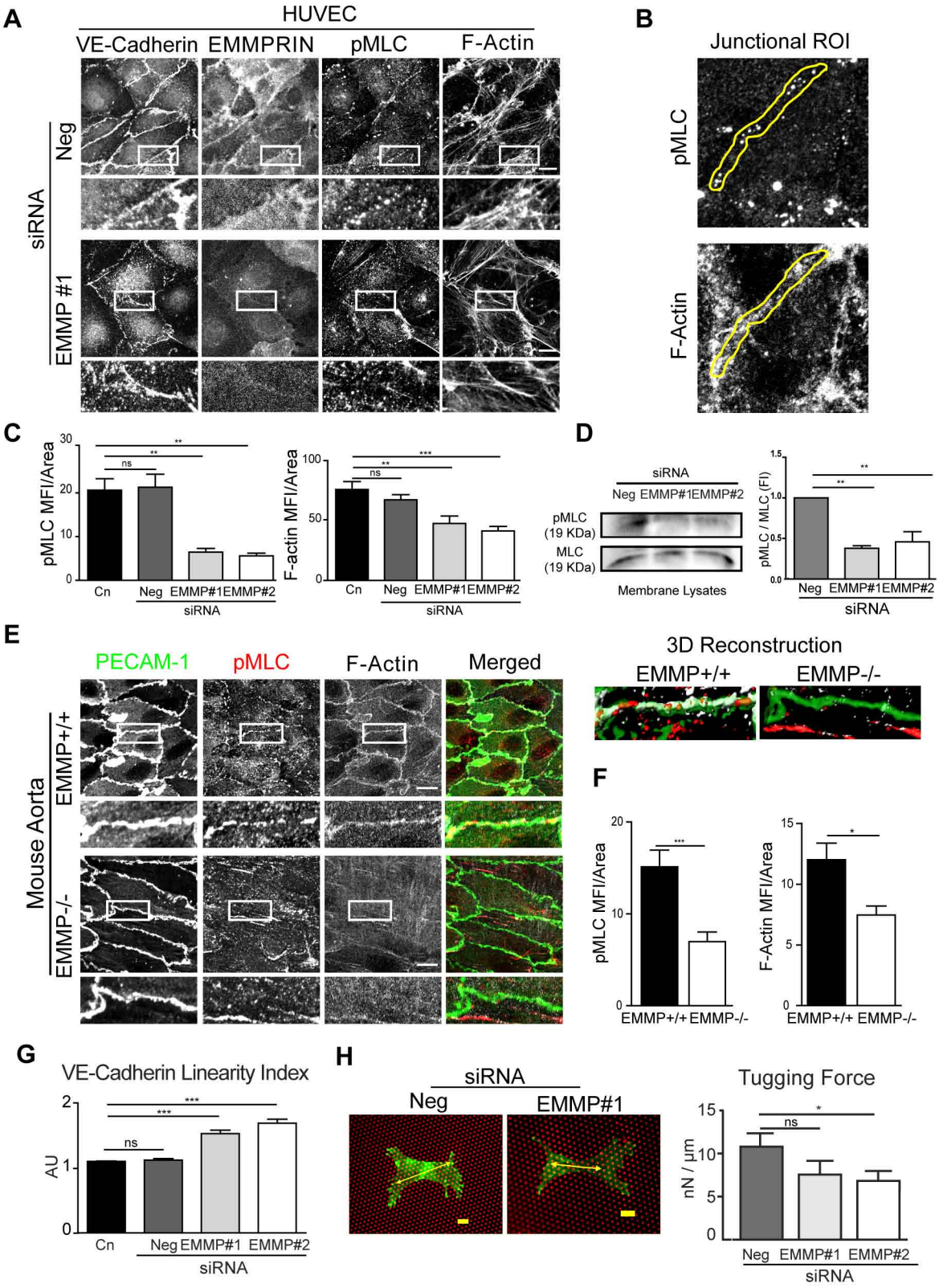

Figure 4

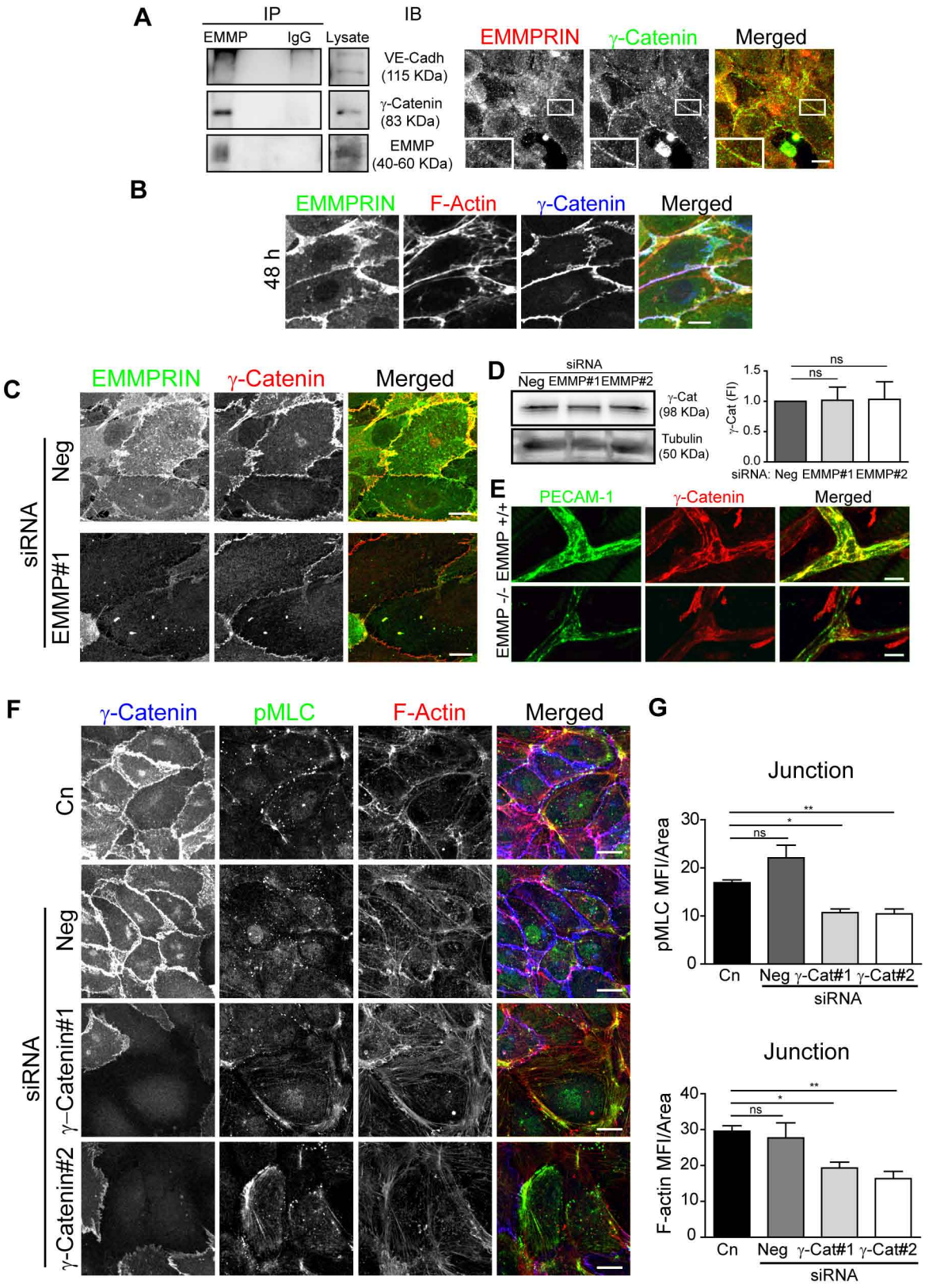

Figure 5

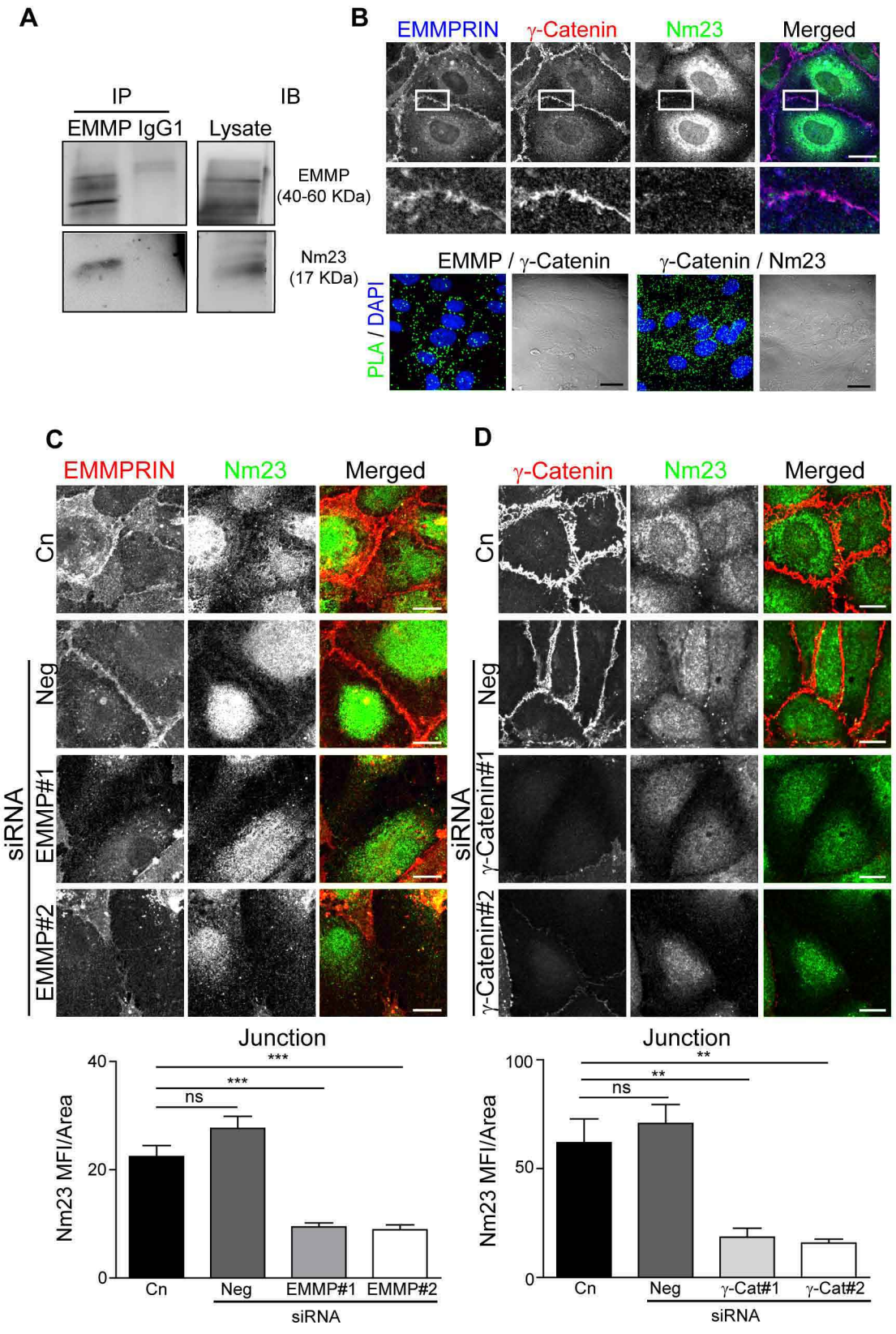

Figure 6

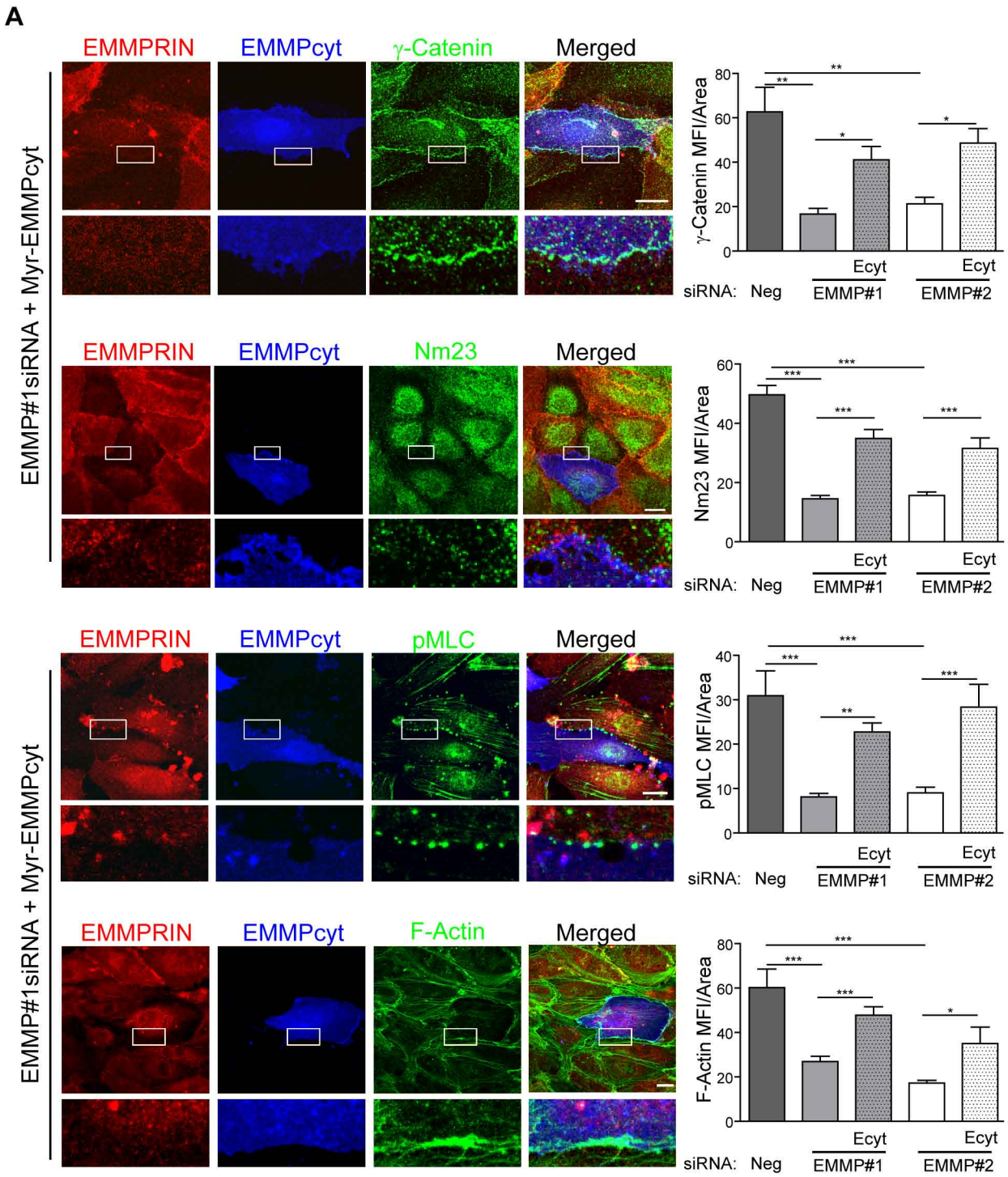

Figure 7

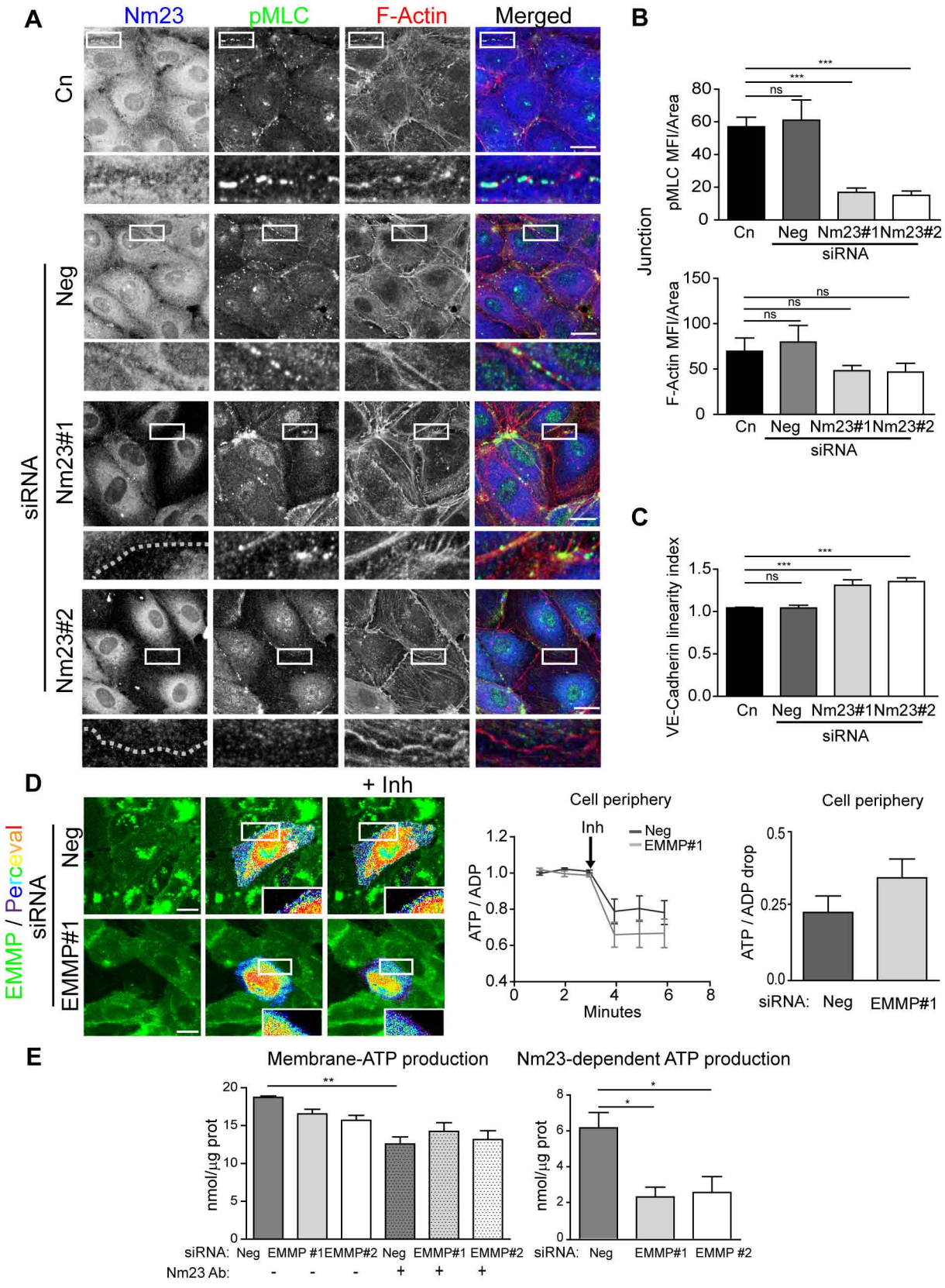

Figure 8